Electronic structure and de Haas–van Alphen frequencies in KFe$_2$As$_2$ within LDA+DMFT

Electronic structure and de Haas–van Alphen frequencies in KFe$_2$As$_2$ within LDA+DMFT

Steffen Backes, Daniel Guterding, Harald O Jeschke and Roser Valentí

Institut für Theoretische Physik, Goethe-Universität Frankfurt, Max-von-Laue-Str. 1, D-60438 Frankfurt am Main, Germany

E-mail: backes@itp.uni-frankfurt.de and valenti@itp.uni-frankfurt.de

Abstract

Recent density functional theory (DFT) calculations for KFe$_2$As$_2$ have been shown to be insufficient to satisfactorily describe angle-resolved photoemission (ARPES) measurements as well as observed de Haas–van Alphen (dHvA) frequencies. In the present work, we extend DFT calculations based on the full-potential linear augmented plane-wave method by dynamical mean field theory (DFT+DMFT) to include correlation effects beyond the local density approximation. We present results for two sets of reported crystal structures. Our calculations indicate that KFe$_2$As$_2$ is a moderately correlated metal with a mass renormalization factor of the Fe 3d orbitals between 1.6 and 2.7. Furthermore, the obtained shape and size of the Fermi surface are in good agreement with ARPES measurements and we observe some topological changes with respect to DFT calculations such as the opening of an inner hole cylinder at the Z point. As a result, our calculated dHvA frequencies differ greatly from existing DFT results and qualitatively agree with experimental data. On this basis, we argue that correlation effects are important to understand the -presently under debate-nature of the superconducting state in KFe$_2$As$_2$.

Keywords: iron pnictide superconductors, density functional theory, dynamical mean field theory

1. Introduction

KFe_2As_2 is the hole-doped end member of the well-studied $Ba_{1-x}K_xFe_2As_2$ family of iron-based superconductors [1] and it features superconductivity at $T_c = 3.4$ K without the need for application of external pressure [2]. This material is presently under debate since the origin of the superconducting phase and the pairing symmetry are still unclear [3–5], both on the experimental and theoretical sides: recent laser-based angle-resolved photoemission (laser ARPES) measurements found the superconducting order parameter to be of s-wave character with octet line-nodes [6], while a theoretical study [7] based on functional renormalization group considerations predicted a d-wave symmetry in agreement with measurements of thermal conductivity [8]. However, other theoretical studies [9, 10] based on spin pairing theory within the random phase approximation found that s- and d-wave pairing channels are strong competitors in hole-doped Fe-based systems and, therefore, both are possible in KFe_2As_2. Moreover, transport measurements under pressure [11] suggested the presence of a possible phase transition from d-wave to s-wave around 1.75 GPa.

Also, strikingly, quantum oscillation experiments [12] predicted effective charge carrier masses of up to 19 m_e with an average mass enhancement factor m^*/m_{band} of about 9, while estimates from ARPES [13] and cyclotron resonance experiments [14] yield mass enhancements factors of about 3 for certain regions of the Fermi surface. On the theoretical side, density functional theory (DFT) calculations for KFe_2As_2 show poor agreement to ARPES data [13, 15, 16] and to de Haas–van Alphen (dHvA) frequencies [12, 17]. However, an existing DFT+DMFT study [18] for KFe_2As_2 suggested an improved comparison of the Fermi surface contour at $k_z = 0$ with ARPES observations.

The importance of correlations in Fe-based superconductors has been pointed out in the past by numerous studies. A method that has proven to be quite successful in capturing the essential features of this class of correlated metals is DFT+DMFT [18–24]. Since accurate knowledge of the electronic structure is essential for understanding both the normal and the superconducting state in Fe-based superconductors, we perform here a comprehensive LDA +DMFT investigation focused on features of the KFe_2As_2 compound that have not been dealt with in past studies [18]. We critically benchmark our theoretical results with ARPES and dHvA measurements to see in which way these results can improve our current understanding of this system.

2. Methods

We combine DFT with dynamical mean-field theory in order to investigate the electronic structure and the resulting dHvA frequencies of KFe_2As_2. Our calculations are based on the experimentally determined tetragonal $I\ 4/mmm$ structures of KFe_2As_2 by Tafti *et al* [25], which are given for pressure values starting at 0.23 GPa. We obtained a structure at zero pressure by linear extrapolation of the available data points. A comparison of this structure to the existing crystal structure by Rosza and Schuster [26] used in previous theoretical investigations shows that while lattice parameters a, b, and c are consistent, the As z position differs significantly between both structures. The As z position was consistently determined over a large pressure range in the above mentioned study by Tafti *et al* [25] and the As z position determined by Rosza and Schuster does not follow the trend shown by those data. Here we use the new

structure with the following parameters: $a = b = 3.8488$ Å, $c = 13.883$ Å, fractional As $z = 0.140663$. In the appendix we also present results for the Rosza and Schuster [26] structure.

For the DFT calculation we employed the full-potential linear augmented plane-wave framework as implemented in WIEN2k [27], using the local density approximation (LDA) as well as the generalized gradient approximation (GGA) by Perdew, Burke and Ernzerhof [28] to the exchange-correlation functional. These calculations were converged self-consistently on a grid of 726 k points in the irreducible Brillouin zone. We performed calculations both, without and with inclusion of spin–orbit coupling (SO).

In order to include the effect of local correlations we performed fully charge self-consistent DMFT calculations, using modified routines from the WIEN2K code. The projection from Bloch eigenstates to the correlated Fe 3d orbitals was carried out with our implementation [29] of the projection method as described by Aichhorn *et al* [30]. The energy window for the projection onto the localized basis was chosen comparatively large, ranging from -5 eV to 13 eV to capture the higher energy contribution of the Fe 3d orbitals to the density of states arising from the hybridization with the As 4p orbitals.

The DMFT impurity problem was solved using the continuous-time hybridization expansion quantum Monte Carlo solver as implemented in the ALPS [31] code. We employed the Legendre polynomial representation [32] of the Green's function and improved estimators for the self-energy [33]. About 6×10^6 Monte-Carlo sweeps were performed at an inverse temperature $\beta = 40$ eV^{-1}, corresponding to room temperature. The interaction parameters U and J were chosen as $U = 4$ eV and $J = 0.8$ eV in terms of Slater integrals F^0, F^2 and F^4, where for the Fe 3d-electrons we used $U = F^0$, $J = (F^2 + F^4)/14$, and $F^2/F^4 = 0.625$ [34]. As the double-counting correction the fully-localized limit [35, 36] (FLL) was used. All orbital characters presented here are defined in a coordinate system which is rotated by 45° around the crystallographic z axis, *i.e.* x and y are pointing along Fe–Fe nearest neighbour bonds. For determining the LDA+DMFT excitation energies that we used to define the Fermi surface, we tracked the maximum of the real-frequency spectral function throughout the Brillouin-zone. Analytic continuation of imaginary frequency data to the real frequency axis was performed by using the Padé approximation for the impurity self-energy and we checked the results against the stochastic analytic continuation method [37].

Two-dimensional cuts through the Fermi surface were extracted from WIEN2k on 200×200 k point grids for the LDA calculations. The Fermi surface was interpolated linearly.

dHvA frequencies were calculated from the electronic band structure using our own implementation of the dHvA frequency extraction algorithm by Rourke and Julian [38]. Band energies were extracted on grids spanning the reciprocal unit cell with 27648 k points for the DFT(+SO) setups and 50 000 k points for the DMFT calculations. To calculate the dHvA frequencies we first find the area of the Fermi surface, which is directly proportional to the observed experimental dHvA frequencies, on cuts through the Brillouin zone. A supercell in reciprocal space is needed to capture orbits on the Fermi surface, which extend across multiple unit cells. In the present case this happens because the two-dimensional Fermi surface sheets of iron-based superconductors are open in the k_z-direction. If the cut contains the k_z-direction, the area of the Fermi surface will be infinite and not detectable even in the supercell approach. For directions close, but not parallel to the k_z-direction, the resulting orbits will be larger than the reciprocal unit cell, but finite, and hence become detectable in the supercell approach.

Furthermore the supercell approach allows for statistical evaluation of the results over an ensemble of detected orbits. The deviation of the individual frequencies from the mean gives an

estimate of how the discretization of the Fermi surface influences the results. We find this influence to be negligible with the given resolution and interpolation techniques.

The dHvA orbit finding procedure was carried out on a 6.4×10^7 k point supercell grid containing 64 reciprocal unit cells. The higher k point density in the supercell compared to the input files is achieved by tricubic interpolation [39]. We align the supercell with a fictitious magnetic field vector, which allows us to investigate the angular dependence of dHvA frequencies. Here we varied the angle of the magnetic field from the (001) towards the (010) direction in reciprocal space. In order to calculate the dHvA frequencies, the supercell is cut into one k point thick slices perpendicular to the vector of the magnetic field. On these slices a stepping algorithm detects crossings of the Fermi level between grid points and interpolates the position of the Fermi surface linearly. Point ordering is ensured within the stepping algorithm. If a closed orbit is detected, its area can be calculated from the geometry of the points unambiguously. The three-dimensional Fermi surface is reconstructed by matching orbits slice-by-slice. Only extremal orbits are singled out since non-extremal orbits do not contribute in experiment. dHvA frequencies are calculated for the extremal orbits and their positions are matched back to the reciprocal unit cell. Orbits with similar position and frequency are averaged.

3. Results

3.1. Electronic structure

We first investigated the band structure of KFe_2As_2 obtained by the DFT calculation within LDA and LDA+SO. Results obtained with the GGA functional were nearly identical to the LDA result and are therefore not shown. At the Γ point (see figures 1(a) and 2(a)) we see three bands crossing the Fermi level, forming hole pockets of Fe $3d_{xy}$, $3d_{xz}$ and $3d_{yz}$ character. The two outer hole pockets form cylinders along k_z between the Γ and Z points, while the cylinder of the third inner hole pocket closes shortly before Z. This leads to two hole pockets at the Z point, being mostly of Fe $3d_{xy}$, $3d_{xz/yz}$ character. Around the $\bar{M}$ point, we observe very small hole pockets with Fe $3d_{xy}$, $3d_{xz/yz}$ character, where the bands with mostly Fe $3d_{xz/yz}$ character are very shallow right above E_F, which leads to a high sensitivity to input parameters and total electron charge in the calculation.

By including the spin–orbit interaction we observe an overall repulsion between touching or degenerate bands, which leads to clear separation of the hole pockets along the high symmetry directions (see figures 1(c), (d)).

Comparing these DFT results to ARPES measurements [13, 15, 16] we find that the agreement in size and shape of the hole pockets along the high symmetry directions is quite poor. This disagreement has already been noted in the publications cited above. The inner two pockets (α, ζ) are too large while the outer one (β) is too small. The topology of the Fermi surface also differs from experimental observations. ARPES clearly shows a separated outer hole cylinder at Γ, while the two inner ones overlap considerably [13, 15, 16]. The closure of the inner hole cylinder is not seen in ARPES [13, 15, 16] or dHvA [12, 17] measurements, leading to a third inner hole pocket at Z in experiments. Also, the hole pockets (ϵ) close to $\bar{M}$ are too small in DFT.

When including correlations on the Fe 3d orbitals via DMFT, the electronic structure of KFe_2As_2 changes significantly. Dynamical mean-field theory yields very similar results for both
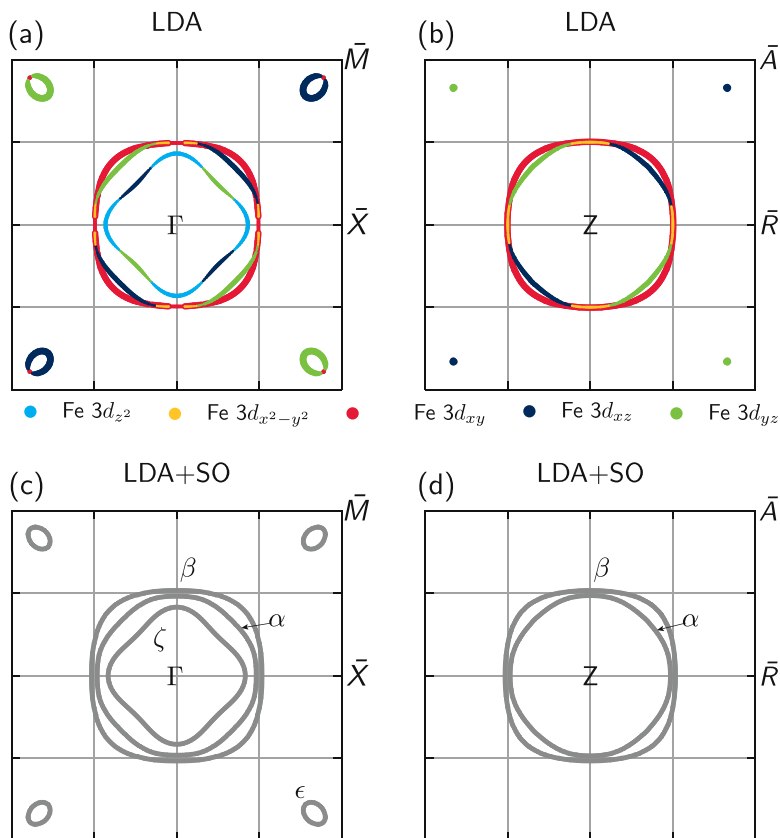
Figure 1. Overview of Fermi surface cuts at $k_z = 0$ and $k_z = \pi$ in KFe$_2$As$_2$ obtained from DFT using the LDA exchange correlation functional with and without spin–orbit coupling (SO). Inclusion of spin–orbit coupling only leads to small quantitative changes, in particular a lifting of all apparent degeneracies of Fermi surface sheets. Fermi surfaces are shown in the two-Fe Brillouin zone representation.

LDA and GGA initial calculations of the electronic structure. In what follows we present the LDA+DMFT results. In the band structure shown in figure 2 we observe a strong renormalization of the bands around the Fermi level, with mass enhancements for the Fe 3d orbitals ranging from 1.56 to 2.72, as shown in table 1.

These results are in agreement with a previous LDA+DMFT study [18], but still very different from experimentally reported mass enhancements, that can reach values of up to 24 for the small pockets (ϵ) and up to 6.9 for the large pockets (α, β, ζ) in the centre of the reciprocal unit cell [12, 17]. We attribute the discrepancy between our results and the experimentally observed mass enhancements partly to the restriction of the interactions in our method to be only of density–density type, since it is known that including the full four-index rotationally invariant U-tensor can increase the resulting mass enhancements significantly [19]. Also the inclusion of other effects missing in our current LDA+DMFT method like non-local correlations and electron–phonon interactions should be able to further reduce the differences between theory and experiment. It was already pointed out in [17] that flattening of the bands near the Fermi level caused by coupling to low-energy bosonic excitations [40] that originate from strong spin fluctuations present in KFe$_2$As$_2$ [41–43], also contribute to the mass enhancement, but are not accounted for in the DMFT method. On the other hand overall
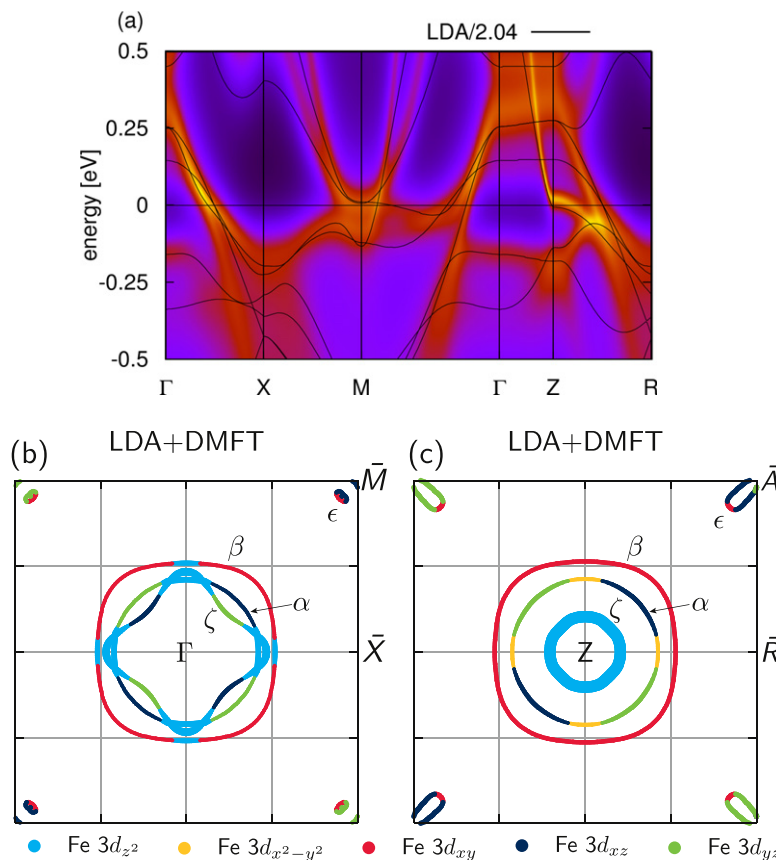
**Figure 2.** The k-resolved spectral function and orbital-resolved Fermi surface of KFe$_2$As$_2$ within LDA+DMFT (see detailed explanation in the text). The LDA bands (black lines) are rescaled by the average mass enhancement of 2.04 for comparison. Dominant orbital characters are indicated by the colour scale. Fermi surfaces are shown in the two-Fe Brillouin zone representation.

Table 1. The orbital-resolved mass enhancements for the Fe 3d orbitals in KFe$_2$As$_2$.

Orbital	d_{xy}	d_z^2	$d_{x^2-y^2}$	$d_{xz/yz}$
$\dfrac{m^*}{m_{LDA}}$	2.72	1.89	1.56	2.02

bandwidth renormalization as seen in ARPES, which is independent of such low-energy bosonic excitations, is well reproduced in DMFT. Therefore, our results support the interpretation given in [17].

We also observe a reordering of bands along the high symmetry directions with significant changes in the size of the hole cylinders. Both the inner sheets (α, ζ) at the Γ point at $k_z = 0$ shrink in size, while the outer one (β) gets enlarged, as seen in the LDA+DMFT Fermi surface in figure 2. This is in better agreement with experimental observations. Moreover, we observe a small overlap of the centre (ζ) and middle hole pocket (α) with small intersection nodes around Γ, which are also observed in ARPES but were absent in the DFT calculation and previous LDA+DMFT studies [18]. Most importantly, at $k_z = \pi$ around the Z point the band of mostly
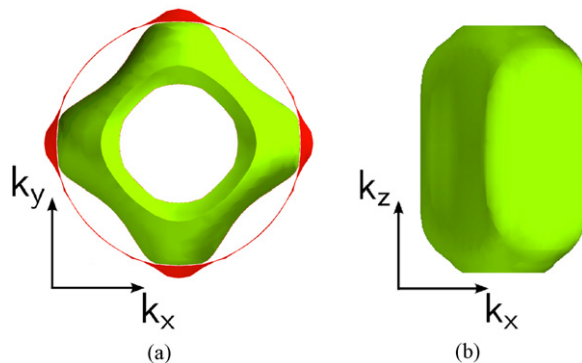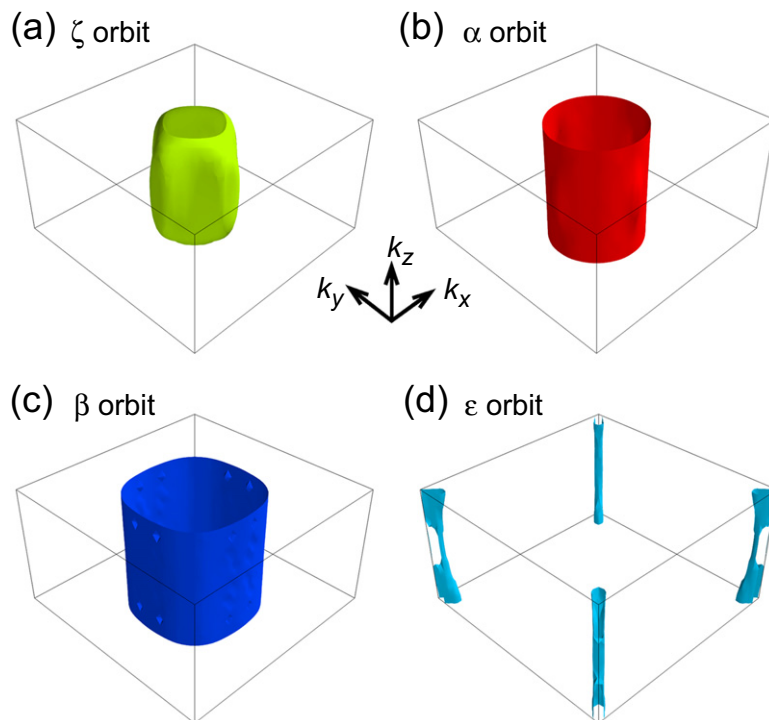
Figure 3. Three dimensional view of the Fermi surface obtained from LDA+DMFT in the two-Fe Brillouin zone representation. (a) Shows the intersection nodes between the inner (green) and middle (red) Fermi surface sheet. The configuration used in calculating de Haas–van Alphen frequencies is indicated by the colours. (b) Shows the dispersion of the inner Fermi surface sheet along the k_z-axis.

$3d_{z^2}$ character that was located just below the Fermi level is pushed above E_F due to correlations, opening the hole cylinder that was previously closed in the DFT calculation. By also investigating the structure from Rosza and Schuster [26], we found a strong dependence of the shape of this hole pocket on the As-z position (see appendix). Within DFT alone, an opening of a new hole pocket can be observed by increasing the As height above the Fe plane. Since the band in question originates from the hybridization of Fe 3d with As 4p states, it is extremely sensitive to the arsenic position. The LDA+DMFT middle hole pocket around Z reduces in size compared to LDA, forming an almost k_z-dispersionless hole cylinder between the Γ and Z points. In figures 3 and 4 we show three-dimensional plots of the hole cylinders throughout the Brillouin zone.

Recent ARPES experiments [13, 15, 16] and dHvA measurements [12, 17] also observe three hole pockets around the Z point, agreeing well with our calculations. The strong Fe $3d_{z^2}$ character around Z reported from ARPES [16] is also reproduced by our calculation. A detailed comparison shows, however, still some differences between theory and ARPES experiment: the size of the middle hole pocket in the k_x–k_y-plane at both the Γ and Z points is smaller in ARPES, while the inner pocket at Z seems to be larger compared to our results.

The small hole pockets at the $\bar{M}$ point emerge from the crossing of two bands at an energy of about 5 meV above E_F, with very weak dispersion of one of the bands. Therefore, these pockets are extremely sensitive to the Fermi level which makes them strongly dependent on the details of the calculation like the double-counting scheme or the chosen DFT functional. On the experimental side this indicates a strong dependence on the actual composition and possible impurities in the sample; this is a possible explanation for the different sizes of these pockets in ARPES experiments [13, 15, 16]. In the appendix we show that for the structure by Rosza and Schuster [26] we indeed observe larger hole pockets at the $\bar{M}$ point compared to results for the structure of Tafti *et al* [25]. In our calculations, we carefully checked the results for different double-counting procedures and analytic continuation methods and found overall qualitatively good agreement. Finally, we note that in order to obtain a better agreement with experiment, the middle hole cylinder would have to be shifted inside of the inner cylinder in our calculations. This cannot be achieved by inclusion of local correlations only since in this system the

Figure 4. Three dimensional view of the Fermi surface obtained from LDA+DMFT in the two-Fe Brillouin zone representation. (a) Shows the sheet that we attribute to the ζ orbit observed in de Haas–van Alphen experiments. (b) Shows the cylinder attributed to the α orbit. (c) Shows the cylinder attributed to the β orbit. The small cusps are artefacts from the technical procedure that we carefully exclude in de Haas–van Alphen calculations. (d) Shows the sheets that we attribute to the ϵ orbits.

necessary shifts of the band energies cannot be obtained with a *k*-independent self-energy only. Instead, a *k*-dependent shift would be required to improve the agreement of the position of the middle hole cylinder at Γ with experiments while retaining the otherwise satisfactory agreement at other *k*-points.

The Fermi surface obtained from LDA+DMFT offers a natural explanation for the magnetic breakdown junctions between orbits α and ζ observed by Terashima *et al* and it [12, 17]. Taking SO into account will likely lift the exact degeneracies at the intersection nodes as seen in our LDA+SO calculation. A shift of the maxima of the spectral function however does not forbid transition processes between Fermi surface sheets if the spectral weight between them remains finite. We conclude that the degeneracy of the lines found in ARPES might be due to both experimental resolution and overestimation of the distance between sheets in our calculation. Furthermore we would like to point out that our Fermi surface strongly resembles the octet line-node structure observed in laser ARPES measurements of the superconducting order parameter [6].

3.2. dHvA effect

Comparing our findings to measurements of quantum oscillations [17] we can confirm that DFT is not able to describe the Fermi surface of KFe_2As_2 correctly. An overview of our results is
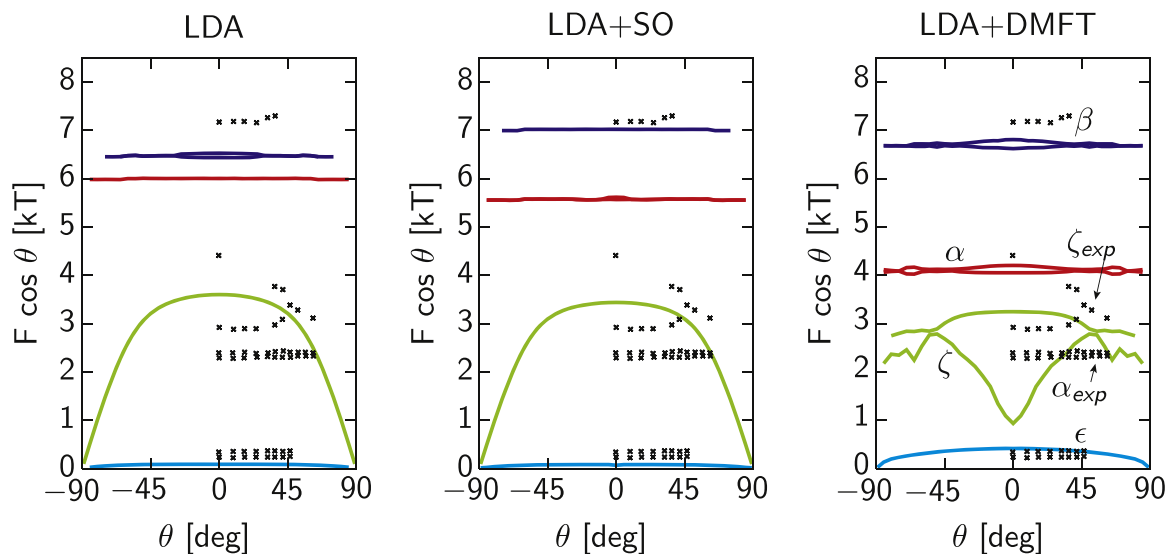
Figure 5. Overview of de Haas–van Alphen frequencies in KFe$_2$As$_2$ calculated from density functional theory and dynamical mean-field theory. Lines represent our calculations, while crosses represent experimental frequencies taken from [17]. Colour coding is the same as in figure 4. The ζ-orbit (innermost) is shown in green, while the frequencies originating from the middle sheet (α) are shown in red. The outermost orbits (β, ϵ) are drawn in blue.

presented in figure 5. LDA and LDA+SO calculations for the structure by Rosza and Schuster are given in the appendix. They reproduce the DFT results by Terashima *et al* [12, 17].

The two inner hole pockets (α, ζ) around the Γ point are too large compared to experimental frequencies, while the outermost hole pocket (β) is too small (figure 5, left panel). The size of the hole pocket close to $\bar{M}$ (ϵ) is already well described in DFT. Adding SO already shows the correct tendency to increase the size of the outer hole pocket and decrease the size of the two inner hole pockets. Deviations from experimentally observed frequencies are nevertheless large (figure 5, middle panel). The good agreement with experiment for the largest and smallest frequencies comes with persisting disagreement for the two intermediate frequencies.

In the LDA+DMFT calculation (figure 5, right panel) the two innermost orbits (α, ζ) intersect around the Γ point (figure 2). For the analysis of the dHvA frequencies we take into account the outermost and innermost possible configuration of these two orbits as shown in figure 4. The same configuration was attributed to fundamental frequencies observed in dHvA experiment [12, 17]. The outer hole pocket (β) is considerably enlarged. As the corresponding electronic band is flattened, it becomes susceptible to tiny energy shifts. Both inner hole pockets (α, ζ) are shifted to lower frequencies and thus decreased in size. The small orbit (ϵ) close to $\bar{M}$ is enlarged around the Z point, but decreases in size around Γ as shown in figure 2. Therefore we only find the maximum frequency for this sheet.

We would like to note that quantum oscillation experiments [44] and ARPES [13, 16] reported the existence of a fourth very small pocket centred at the Z point which was not seen in our calculations for the most recent structure. This fourth pocket is however present in the DFT calculation when using the structure from Rosza and Schuster [26], but we found it to vanish when adding correlations in LDA+DMFT, depending on the double-counting (see appendix).

Table 2. De Haas–van Alphen frequencies in kT (kiloTesla) for $B \parallel (001)$ obtained from DMFT calculations compared to experimental values [17].

	ϵ_l	ϵ_h	α_l	α_h	ζ_l	ζ_h	β_l	β_h
Exp.	0.24	0.36	2.30	2.39	2.89	4.40	7.16	—
LDA+DMFT	—	0.42	4.05	4.20	0.94	3.25	6.62	6.81

Table 3. Electron orbit averaged effective masses in m_e for $B \parallel (001)$ obtained from DMFT calculations compared to experimental values [17].

	ϵ_Γ	ϵ_Z	α_Γ	α_Z	ζ_Γ	ζ_Z	β_Γ	β_Z
Exp.	6.0	7.2	6.0	6.5	8.5	18.0	19.0	19.0
LDA+DMFT	–	5.9	3.4	4.6	2.4	5.3	8.3	8.3

The opening of the innermost hole pocket ζ is clearly observed in the LDA+DMFT calculated dHvA frequencies by the appearance of a lower extremal frequency. As pointed out before in the ARPES section, the middle hole cylinder would have to be decreased in size considerably to match the experimental frequencies. This would in turn increase the enclosed volume of the sheet labelled ζ and thus shift it toward experimentally observed values. A comparison of experimental and LDA+DMFT frequencies for $B \parallel (001)$ is given in table 2.

Furthermore we calculated effective masses averaged over extremal orbits on the Fermi surface from the LDA+DMFT excitation energies. These masses correspond to the effective masses observed in dHvA experiments (table 3). Note that values given in this table are *absolute* masses in contrast to mass *enhancements* given in table 1.

Qualitatively our calculation captures the trends that are observed in sheet-resolved effective masses, however, as discussed above, the differences might be attributed to the restriction to density–density type interactions and effects originating from other than electron–electron interactions missing in DMFT, which increase effective masses seen in dHvA experiments such as electron–phonon coupling.

For comparison with dHvA experiment, we have obtained the Fermi surface within LDA +DMFT by tracing the maxima of the spectral function throughout the Brillouin zone. This approach is insensitive to the broadening of the excitation energies. Experimentally observed dHvA frequencies correspond to orbits with extremal areas and maximal spectral weight, which we take into account with our method. Fermi surface plots generated from the maxima of the spectral function can however mask the true extent of the Fermi surface pockets as seen in ARPES experiments. To allow for a better comparison with ARPES experiments and to visualize the broadening of the excitation energies, we show the orbital resolved spectral function at the chemical potential in figure 6. Compared to the Fermi surface in figure 2 a strong broadening of the bands can be observed, especially in the Fe $3d_{xy}$ and $3d_{xz/yz}$ orbitals. This is in correspondence with the fact that these orbitals also have the strongest renormalization in LDA +DMFT. The small pockets at the $\bar{M}$ point can be seen to represent a very extended structure with no well defined maxima. Note that in the Fermi surface plot obtained using spectral function maxima (figures 2(b) and (c)) the true extent of these pockets is not properly accounted for. From this we conclude that the spectral function in LDA+DMFT (figure 6) is better suited for comparison with photoemission experiments.
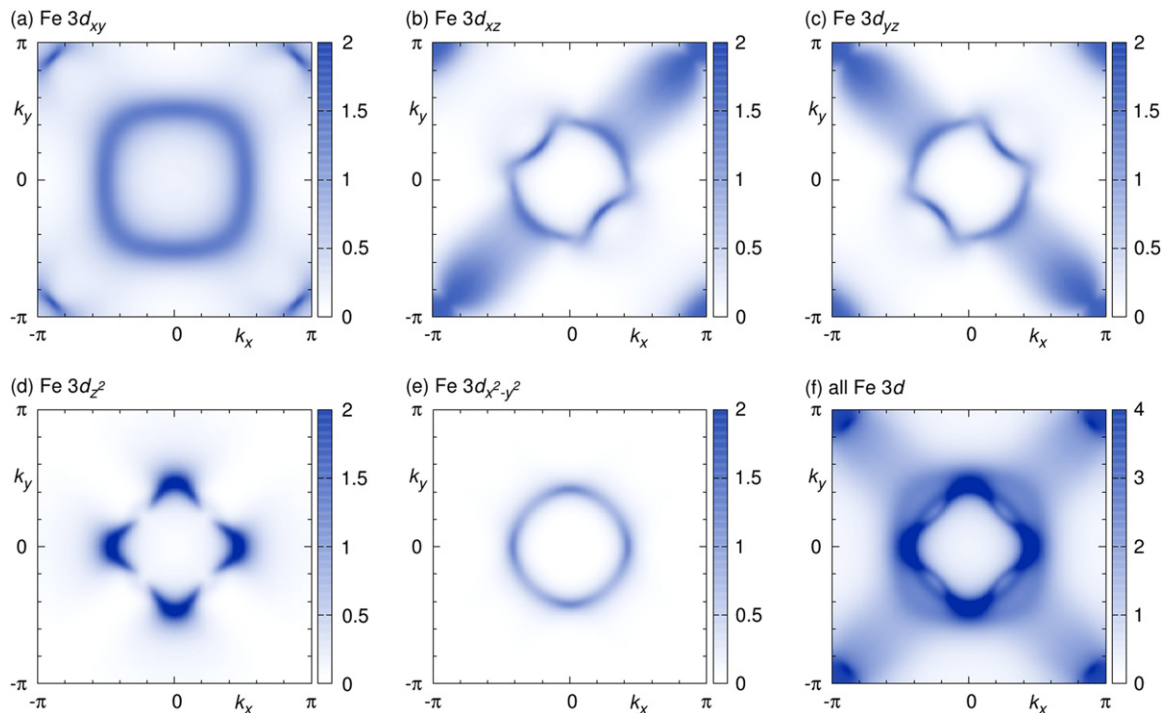
Figure 6. The orbital-resolved spectral function of KFe_2As_2 at $k_z = 0$ and $E = 0$ for the structure by Tafti *et al* [25]. The colour intensity indicates the value of the spectral function. Subfigure (f) shows the summed Fe 3d orbital contributions to the spectral function.

4. Conclusion

In this paper we presented combined DFT with dynamical mean-field theory calculations of the Fermi surface and dHvA frequencies in KFe_2As_2. We first showed that DFT calculations with LDA or GGA exchange correlation functionals, with or without SO fail to reproduce the experimentally observed electronic structure of KFe_2As_2.

Most notably, DFT predicts no third inner hole pocket at the Z point, which we find to open in our LDA+DMFT calculation in agreement with experiment. We also obtain a qualitatively correct k_z dispersion of the iron bands, where between the Γ and Z points the dispersion of the inner hole cylinder is greatly increased while the middle hole cylinder shows almost no dispersion, giving a much better agreement with dHvA measurements when identifying them in different order in experiment.

The intersection nodes we found on the inner two hole cylinders offer a natural explanation for magnetic breakdown orbits observed in dHvA measurements [17].

The obtained effective mass-enhancements about $1.6 - 2.7$ show that KFe_2As_2 is a moderately correlated metal and thus a DFT calculation fails to capture the important features that lead to the experimentally observed electronic structure. This has strong implications for the obtained dHvA frequencies, where LDA+DMFT gives distinctively different results than DFT. Our results are in better agreement with both ARPES [13, 16] and quantum oscillation [12, 17] experiments. The observed strong flattening of electronic bands gives a possible explanation for the spread of experimental results in this compound in terms of extreme
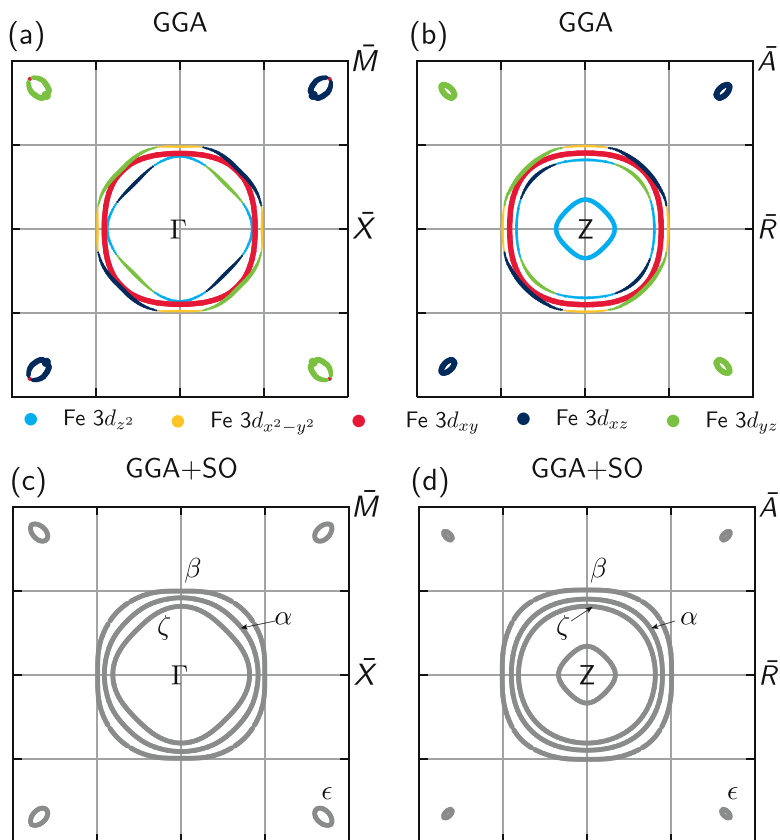
Figure A.1. The orbital-resolved Fermi surface of KFe_2As_2 within DFT for the structural data by Rosza and Schuster [26]. Dominant orbital characters are indicated by the colour scale. Fermi surfaces are shown in the two-Fe Brillouin zone representation.

sensitivity to the experimental stoichiometry. We conclude that LDA+DMFT captures most of the important correlation effects in KFe_2As_2 and such a treatment may be necessary in order to understand the controversial nature of superconductivity in this system. This will be a subject of future work.

Acknowledgments

## Appendix. Sensitivity analysis of the Fermi surface and dHvA frequencies

Previous theoretical work on KFe_2As_2 was based on the structural data obtained by Rosza and Schuster [26], while new results for elevated pressure by Tafti *et al* [25] became available recently. These structures differ most noticeably in the As z-position, where the old structure
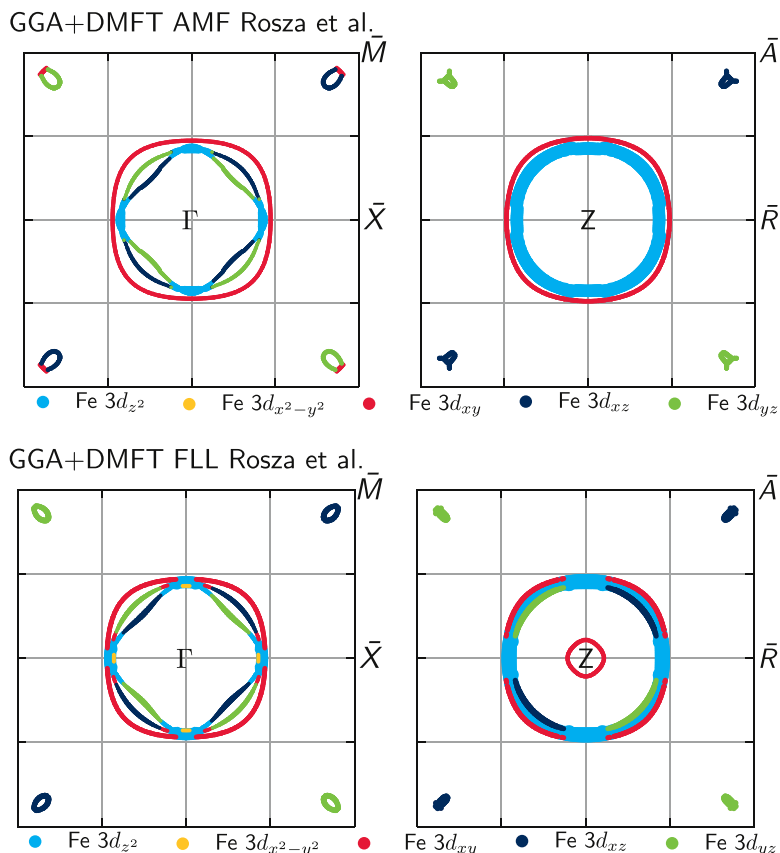
Figure A.2. The orbital-resolved Fermi surface of KFe$_2$As$_2$ within GGA+DMFT using the structural data by Rosza and Schuster [26]. Dominant orbital characters are indicated by the colour scale. Fermi surfaces are shown in the two-Fe Brillouin zone representation. AMF indicates the around mean-field, FLL the fully-localized limit double-counting.

has a fractional coordinate of $z = 0.1475$, while the new one yields $z = 0.140663$ by interpolation to 0 GPa. Therefore, to interpret current theoretical investigations correctly, we investigate the dependence of the Fermi surface and dHvA frequencies of KFe$_2$As$_2$ on the two different structures and also on different double-counting methods within LDA+DMFT. We also tested the dependence of these quantities upon considering LDA versus GGA and found only minor changes. Here we present GGA results.

We find very different behaviour for the two structural configurations: the Fermi surfaces for the Rosza and Schuster [26] structure can be seen in figure A.1, to be compared to the Tafti *et al* [25] structure in figure 1. The cut at $k_z = 0$ is qualitatively identical but the Fermi surface topology at the *Z* point is different, where the structure of Rosza and Schuster with the higher As *z*-position features two additional inner hole pockets around *Z*. The inner one emerges from a small hole pocket centred at *Z*, while the second inner one corresponds to the open ζ-hole cylinder, which closes shortly before $k_z = \pi$ in the structure by Tafti *et al* [25]. From our calculations we can deduce that the As *z*-position is the key factor for the existence of these hole pockets. This makes sense since their main orbital character is either Fe $3d_{z^2}$ or As $4p$, giving rise to a strong dependence on the Fe-As bonding distance. By lowering the As *z*-position, and
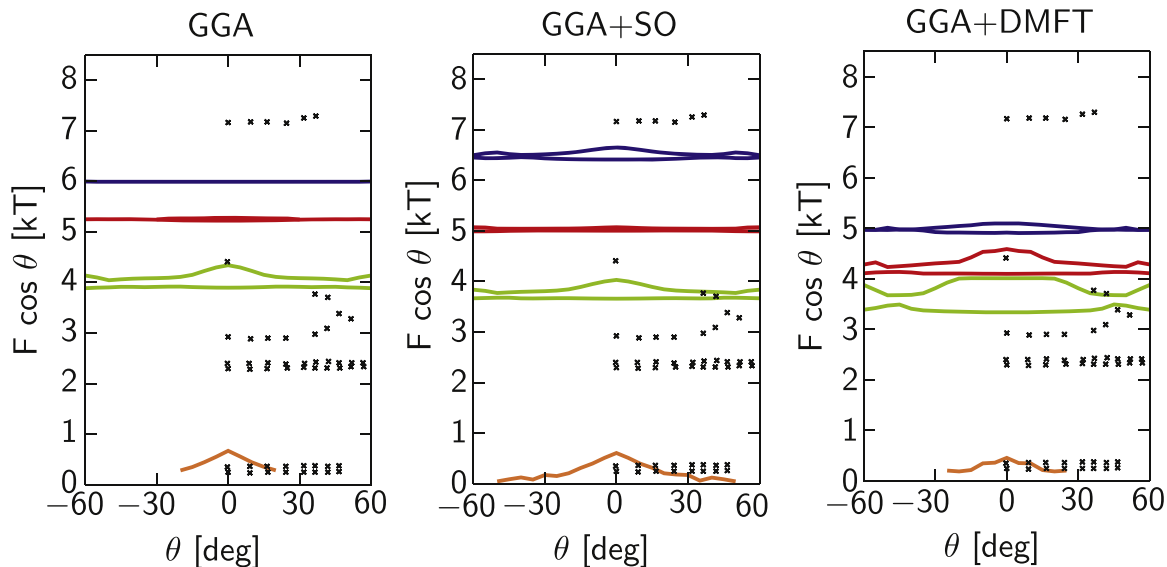
Figure A.3. Overview of de Haas–van Alphen frequencies in KFe$_2$As$_2$ calculated from density functional theory and dynamical mean-field theory with FLL double-counting using the structural data by Rosza and Schuster [26]. Lines represent our calculations, while crosses represent experimental frequencies taken from [17]. Colour coding is the same as in figure 4. The ζ-orbit (innermost) is shown in green, while the frequencies originating from the middle sheet (α) are shown in red. The outermost orbit (β) is drawn in blue. The orbit shown in orange corresponds to a small pocket at the Z point.

thus enhancing the hybridization of the Fe 3d with the As 4p orbitals, the two inner pockets become smaller and finally vanish.

In figure A.2 we show cuts of the Fermi surface in LDA+DMFT, calculated for the structure by Rosza and Schuster. The electronic structure depends on the double-counting correction. With the FLL double-counting the fourth inner hole pocket stays present at the Z point, whereas with the around mean-field (AMF) double-counting it vanishes. This can be explained by the large As 4p character of the inner hole pocket, which makes it sensitive to the double-counting method. Since AMF reduces the self-energy by a smaller degree than FLL, this band is pushed below the Fermi level when using the AMF method. In the structure by Tafti *et al* this band is farther away from the Fermi level already in the DFT calculation, lowering the As 4p contribution to the density of states at E_F. Therefore, we see only slight differences between the two double-counting corrections in the Tafti *et al* structure without qualitative changes. In figure A.3 we show the dHvA frequencies for the structure by Rosza and Schuster. The small orbits at the $\bar{M}$ point are not shown as they give very low frequencies.

References

[1] Rotter M, Pangerl M, Tegel M and Johrendt D 2008 Superconductivity and crystal structures of (Ba$_{1-x}$K$_x$) Fe$_2$As$_2$ (x = 0-1) *Angew. Chem. Int. Ed.* **47** 7949
[2] Kihou K *et al* 2010 Single crystal growth and characterization of the iron-based superconductor KFe$_2$As$_2$ synthesized by KAs flux method *J. Phys. Soc. Japan* **79** 124713

[3] Wang F and Lee D-H 2011 The electron pairing mechanism of iron-based superconductors *Science* **332** 200–4

[4] Hirschfeld P J, Korshunov M M and Mazin I I 2011 Gap symmetry and structure of Fe-based superconductors *Rep. Prog. Phys.* **74** 124508

[5] Chubukov A V 2012 Pairing mechanism in Fe-based superconductors *Annu. Rev. Condens. Matter Phys.* **3** 57–92

[6] Okazaki K *et al* 2012 Octet-line node structure of superconducting order parameter in KFe_2As_2 *Science* **337** 1314

[7] Thomale R, Ch Platt, Hanke W, Hu J and Bernevig B A 2011 Exotic d-wave superconducting state of strongly hole-doped $K_xBa_{1-x}Fe_2As_2$ *Phys. Rev. Lett.* **107** 117001

[8] Reid J-Ph *et al* 2012 Universal heat conduction in the iron arsenide superconductor KFe_2As_2: evidence of a d-wave state *Phys. Rev. Lett.* **109** 087001

[9] Maiti S, Korshunov M M, Maier T A, Hirschfeld P J and Chubukov A V 2011 Evolution of the superconducting state of Fe-based compounds with doping *Phys. Rev. Lett.* **107** 147002

[10] Suzuki K, Usui H and Kuroki K 2011 Spin fluctuations and unconventional pairing in KFe_2As_2 *Phys. Rev. B* **84** 144514

[11] Tafti F F, Juneau-Fecteau A, Delage M-È, René de Cotret S, Reid J-Ph, Wang A F, Luo X-G, Chen X H, Doiron-Leyraud N and Taillefer L 2013 Sudden reversal in the pressure dependence of T_c in the iron-based superconductor KFe_2As_2 *Nat. Phys.* **9** 349

[12] Terashima T *et al* 2010 Fermi surface and mass enhancements in KFe_2As_2 from de haas-van alphen effect measurements *J. Phys. Soc. Japan* **79** 053702

[13] Yoshida T *et al* 2011 Fermi surfaces and quasi-particle band dispersions of the iron pnictide superconductor KFe_2As_2 observed by angle-resolved photoemission spectroscopy *J. Phys. Chem. Solids* **72** 465

[14] Kimata M *et al* 2011 Cyclotron resonance and mass enhancement by electron correlation in KFe_2As_2 *Phys. Rev. Lett.* **107** 166402

[15] Sato T *et al* 2009 Band structure and fermi surface of an extremely overdoped iron-based superconductor KFe_2As_2 *Phys. Rev. Lett.* **103** 047002

[16] Yoshida T *et al* 2014 Orbital character and electron correlation effects on two- and three-dimensional Fermi surfaces in KFe_2As_2 revealed by angle-resolved photoemission spectroscopy *Front. Phys.* **2** 17

[17] Terashima T *et al* 2013 Fermi surface in KFe_2As_2 determined via de Haas–van Alphen oscillation measurements *Phys. Rev. B* **87** 224512

[18] Yin Z P, Haule K and Kotliar G 2011 Kinetic frustration and the nature of the magnetic and paramagnetic states in iron pnictides and iron chalcogenides *Nat. Mater.* **10** 932

[19] Aichhorn M, Biermann S, Miyake T, Georges A and Imada M 2010 Theoretical evidence for strong correlations and incoherent metallic state in FeSe *Phys. Rev. B* **82** 064504

[20] Hansmann P, Arita R, Toschi A, Sakai S, Sangiovanni G and Held K 2010 Dichotomy between large local and small ordered magnetic moments in iron-based superconductors *Phys. Rev. Lett.* **104** 197002

[21] Aichhorn M, Pourovskii L and Georges A 2011 Importance of electronic correlations for structural and magnetic properties of the iron pnictide superconductor LaFeAsO *Phys. Rev. B* **84** 054529

[22] Ferber J, Foyevtsova K, Valentí R and Jeschke H O 2012 LDA + DMFT study of the effects of correlation in LiFeAs *Phys. Rev. B* **85** 094505

[23] Ferber J, Jeschke H O and Valentí R 2012 Fermi surface topology of LaFePO and LiFeP *Phys. Rev. Lett.* **109** 236403

[24] Werner P, Casula M, Miyake T, Aryasetiawan F, Millis A J and Biermann S 2012 Satellites and large doping and temperature dependence of electronic properties in hole-doped $BaFe_2As_2$ *Nat. Phys.* **8** 331

[25] Tafti F F *et al* 2014 Sudden reversal in the pressure dependence of T_c in the iron-based superconductor $CsFe_2As_2$: a possible link between inelastic scattering and pairing symmetry *Phys. Rev. B* **89** 134502

[26] Rosza S and Schuster H U 1981 *Z. Naturforsch.* B **36** 1668

[27] Blaha P, Schwarz K, Madsen G K H, Kvasnicka D and Luit J 2001 WIEN2k *An Augmented PlaneWave +LocalOrbitals Program for Calculating Crystal Properties* (Vienna: Techn. Universität Wien)

[28] Perdew J P, Burke K and Ernzerhof M 1996 Generalized gradient approximation made simple *Phys. Rev. Lett.* **77** 3865

[29] Ferber J, Foyevtsova K, Jeschke H O and Valentí R 2014 Unveiling the microscopic nature of correlated, organic conductors: the case of κ-(BEDT-TTF)$_2$Cu(N(CN)$_2$)Br$_x$Cl$_{1-x}$ *Phys. Rev.* B **89** 205106

[30] Aichhorn M, Pourovskii L, Vildosola V, Ferrero M, Parcollet O, Miyake T, Georges A and Biermann S 2009 Dynamical mean-field theory within an augmented plane-wave framework: assessing electronic correlations in the iron pnictide LaFeAsO *Phys. Rev.* B **80** 085101

[31] Bauer B *et al* (ALPS Collaboration) 2011 The ALPS project release 2.0: open source software for strongly correlated systems *J. Stat. Mech.* P05001

[32] Boehnke L, Hafermann H, Ferrero M, Lechermann F and Parcollet O 2011 Orthogonal polynomial representation of imaginary-time Green's functions *Phys. Rev.* B **84** 075145

[33] Hafermann H, Patton K R and Werner P 2012 Improved estimators for the self-energy and vertex function in hybridization-expansion continuous-time quantum Monte Carlo simulations *Phys. Rev.* B **85** 205106

[34] Anisimov V I, Aryasetiawan F and Lichtenstein A I 1997 First-principles calculations of the electronic structure and spectra of strongly correlated systems: the LDA+U method *J. Phys*: *Condens. Matter* **9** 767

[35] Anisimov V I, Solovyev I V, Korotin M A, Czyzyk M T and Sawatzky G A 1993 Density-functional theory and NiO photoemission spectra *Phys. Rev.* B **48** 16929

[36] Dudarev S L, Botton G A, Savrasov S Y, Humphreys C J and Sutton A P 1998 Electron-energy-loss spectra and the structural stability of nickel oxide: an LSDA+U study *Phys. Rev.* B **57** 1505

[37] Beach K S D 2004 *Identifying the Maximum Entropy Method as a Special Limit of Stochastic Analytic Continuation* arXiv:cond-mat/0403055

[38] Rourke P M C and Julian S R 2012 Numerical extraction of de Haas-van Alphen frequencies from calculated band energies *Comput. Phys. Commun.* **183** 324

[39] Lekien F and Marsden J 2005 Tricubic interpolation in three dimensions *Int. J. Numer. Meth. Eng.* **63** 455

[40] Ortenzi L, Cappelluti E, Benfatto L and Pietronero L 2009 Fermi-surface shrinking and interband coupling in iron-based pnictides *Phys. Rev. Lett.* **103** 046404

[41] Lee C H *et al* 2011 Incommensurate spin fluctuations in hole-overdoped superconductor KFe$_2$As$_2$ *Phys. Rev. Lett.* **106** 067003

[42] Hirano M *et al* 2012 Potential antiferromagnetic fluctuations in hole-doped iron-pnictide superconductor Ba$_{1-x}$K$_x$Fe$_2$As$_2$ studied by ^{75}As nuclear magnetic resonance measurement *J. Phys. Soc. Japan* **81** 054704

[43] Zhang S W, Ma L, Hou Y D, Zhang J, Xia T-L, Chen G F, Hu J P, Luke G M and Yu W 2010 ^{75}As NMR study of single crystals of the heavily overdoped pnictide superconductors Ba$_{1-x}$K$_x$Fe$_2$As$_2$ ($x = 0.7$ and 1) *Phys. Rev.* B **81** 012503

[44] Zocco D A, Grube K, Eilers F, Wolf T and v Löhneysen H 2014 Fermi surface of KFe$_2$As$_2$ from quantum oscillations in magnetostriction *J. Phys. Soc. Japan Conf. Proc.* **3** 015007